Electronic Properties of BZT Nano-Ceramic Grades at Low Frequency Region

Darko Kosanović[1*)], Vladimir A. Blagojević[2], Stanko O. Aleksić[3], Jelena Živojinović[1], Adriana Peleš Tadić[1], Vladimir B. Pavlović[4], Nina Obradović[1]

[1]Institute of Technical Sciences of the Serbian Academy of Sciences and Arts, Knez Mihailova 35/IV, Belgrade, 11000, Serbia
[2]TBP Sotfware, Ilije Garašanina 4/4, Beograd
[3]Institute Iritel, Batajnički put 23, 11 000 Belgrade
[4]Faculty of Agriculture, University of Belgrade, Nemanjina 6, 11080, Belgrade-Zemun, Serbia

Abstract:

BZT ceramics was prepared by using fine powder mixture of $BaCO_3$, TiO_2 and ZrO_2 in the respective molar ratio to form $Ba(Zr_{0.10}Ti_{0.90})O_3$ via solid state reaction at elevated temperature. The prepared BZT was milled in the planetary ball mill from 0-120 min to achieve different powder grades from micron to nano-sized particles. After the powder characterization by XRD and SEM the samples were pressed in disc shape and sintered at different temperatures from 1100-1350°C in the air. The sintered samples were characterized by SEM and their density and average grain size was determined and presented vs. sintering temperature and powder grades (milling time). After that the silver epoxy electrodes were deposited on sintered disc samples. The disc samples capacity and resistivity were measured at low frequency region from 1 Hz to 200 kHz using low frequency impedance analyzer. The sintering temperatures and powder grades were used as parameters. Finally the specific resistance ρ, dielectric constant (ε' + jε'') and tgδ where determined from the impedance measurements. The behavior of electronic properties where analyzed e.g. the relaxation effect of the space charge (inter-granular electric charges) vs. sintering temperature and ceramic grades. The results obtained were compared with best literature data for the losses in BZT ceramics at low frequencies.

Keywords: BZT ceramics; Sintering; Dielectric Properties.

1. Introduction

In the last few years, the dielectric and optical properties of relaxer ferroelectrics have been widely investigated for applications in wireless communications, metal–oxide–semiconductor field-effect transistors, and optical and microwave dielectrics [1-6]. The main characteristics of relaxer ferroelectrics are the large, temperature dependent, diffuse and frequency dispersive maximum of relative permittivity (ε) [7].

Ferroelectric materials with perovskite type structure (ABO_3) have been studied extensively, because of their broad technical application in memory storage devices, multilayer ceramic capacitors (MLCC) and piezoelectric devices. Since the 20th century

_____

[*)] **Corresponding author:** darko.kosanovic@itn.sanu.ac.rs

_____

BaTiO$_3$ gained interest due to environmental and fundamental studies [8]. Ba(Zr,Ti)O$_3$ was considered as an important material for ceramic capacitors, because Zr^{4+} is chemically more stable than Ti^{4+}[9].

BaTiO$_3$ itself shows a high dielectric constant with a sharp maximum at about 130°C. With proper dopants this maximum can be depressed and shifted resulting in a stable dielectric over a wide temperature range. Solid solution of BaTiO$_3$ doped with Zr^{4+} and/or Ca^{2+} offer a higher relative permittivity but in a narrower temperature range. So Ba(Zr,Ti)O$_3$ systems have been established as one of the most important compositions for MLCC [10, 11]. BaTiO$_3$ ceramics gained great interest due to the ferroelectric characteristics. It's low Curie temperature T$_C$ of 120°C sets a limit for high power transducers and the low electromechanical coupling factor is not as interesting as that of PZT. The drawback of pure BaTiO$_3$ is the high temperature coefficient near the Curie temperature. The high temperature coefficient can be avoided by adding dopants due to the shifting of the transition temperature. BaTiO$_3$ shows a multiple ferroelectric-ferroelectric phase transition which results in a temperature dependence of piezoelectric properties. A large piezoelectric coefficient results by a substitution on the Ba^{2+} or Ti^{4+} side. Also a good electromechanical coupling factor and a more stable structure is observed. An important example is Ba(Zr,Ti)O$_3$ which can be used in different devices [12, 13].

Barium strontium titanate (Ba,Sr)TiO$_3$ (BST) with high dielectric constant value combined with low dissipation factor makes BST one of the promising candidates for dynamic random access memory (DRAM) applications. The BST system is well known for it's strong response to the applied dc electric field. This property is very attractive and has been used to develop devices operating in the microwave and millimeter range such as phase shifters, frequency agile filters, and tuneable capacitors [14-17]. Moreover, the substitution of barium by strontium in barium titanate can improve the properties such as lowering the temperature of ferroelectric transformation, increasing dielectric constant, lowering dielectric dissipation and elevating pyroelectric coefficient [18-23]. It is also reported that barium zirconate titanate (BZT) solid solutions are also electric field-tuneable dielectrics with potential use in devices for wireless communications as variable capacitors, phase shifters and voltage-controlled oscillators [24-27].

Currently, barium zirconate titanate Ba(Zr$_x$Ti$_{1-x}$)O$_3$ (BZT) has been chosen as an alternative material to replace barium strontium titanate (Ba,Sr)TiO$_3$ (BST) in the fabrication of ceramic capacitors, since [ZrO$_6$] clusters are chemically more stable than those of [TiO$_6$] [28-32].

Barium zirconate titanate (BZT) is one of the most important traditional functional materials with potential applications as piezoelectric transducers, dynamic random access memory (DRAM), tuneable microwave devices, and in electrical energy storage unit [33-36]. With high dielectric constant, it is generally adopted in Y5V multilayer ceramic capacitors (MLCC) [37, 38].

In literature the BZT ceramics were prepared through solid state method using a calcinations temperature between 1100 and 1250°C with 2 to 12 h holding time [39-43]. BZT ceramics are usually prepared by conventional sintering at high temperatures of about 1550 °C for several hours with a holding time of 2-8 h [44-47]. The high temperature sintering process leads to the formation of coarse-grained ceramics with substantial grain growth. Furthermore the relative density is determined with 90 to 94 % as Mahesh et al reported [48].The ferroelectricity of BZT ceramics changes with the Zr^{4+} content. Therefore, at higher Zr^{4+} content x > 0.08 show a broad peak by plotting temperature vs. the relative permittivity ε$_r$ due to the inhomogeneous distribution of Zr^{4+}ions in the Ti^{4+} site. With a Zr^{4+} content of x = 0.20 only one phase transition exists and by increasing the content to x = 0.25 the typical relaxer behaviour can be observed [49]. BZT ceramics show a rhombohedral and tetragonal structure in the range of $0.10 \leq x \leq 0.15$. Above that Zr^{4+} content range the structure changes from rhombohedral to cubic [50-53]. Rehrig et al. reported that the BZT ceramic with a low

_____

Zr^{4+} content provide a crystal growth in millimeter size and a piezoelectric coefficient of 355 pC/N is determined at room temperature [52]. In 2015 Yang, Wu et al. pointed out that with a Zr^{4+} content of 6 % the piezoelectric coefficient reaches 420 pC/N with the conventional solid state reaction at 1400^oC for 100 h [54].

It is known that inter-granular electric charge relaxation in electronic ceramics happens at low frequencies and depends on micro/nano structure (grain size), but it was not enough presented in literature. The results from MF frequency region are more often presented in the region from 100 Hz to 100 MHz. However some medical electronic devices and sensors require work in the low frequency region. This was the motivation for us to prepare BZT different ceramic grades and to measure electronic properties at low frequencies and analyze their behavior vs. grain size and density to find out correlations between the measurements (shape of diagrams) and relaxation of inter-granular charges.

2. Materials and Experimental Procedures

Commercially available powders of $BaCO_3$ (E. Merck, Darmstadt), ZrO_2 (99.99 %, Sigma-Aldrich) and TiO_2 (99.99 %, Sigma-Aldrich) was mechanically activated in the ratio ZrO_2 and TiO_2 (10/90) by grinding in a planetary ball-mill (Fritsch Pulverisette) in air for 0, 40, 80 and 120 minutes, at 300 rev/min. Initial mixtures were milled in a ZrO_2 jar (500 cm^3) with ZrO_2 balls that were 10 mm in diameter. The powder to ball weight ratio was 1:30. After performing mechanical activation, the powders were dispersed in distilled water, ultrasonic treated for 20 minutes and dried at 100^oC for 24 h. The powder mixtures were dried and calcined at temperature of 700^oC, for 2 h inside a chamber furnace, after milling.

The samples of the activated and after that which calcined BZT $(Ba(Zr_{0.10}Ti_{0.90})O_3)$ powders were pressed at 6 t/cm^2 (589 MPa). They were sintered in air in a laboratory chamber furnace (Electron) whose maximum temperature is 1600^oC. The samples were placed into the furnace and sintered at a temperature of 1350^oC for 2 h. The heating rate was 10 ^oC/min. The X-ray powder diffraction patterns were obtained using a Rigaku Ultima IV X-ray diffractometer (XRD) instrument in thin film geometry mode with grazing incidence angle of 0.5°, using Ni-filtered CuKα radiation (λ=1.54178 Å). Diffraction data were acquired over the scattering angle 2θ from 10° to 70° with a step of 0.05° and acquisition rate of 2°/min and obtained data were analyzed with PDXL 2 software. The International Centre for Diffraction Data (ICDD) database was used for the detection of crystal phases.

The morphology and microstructure of sintered BZT powders were analyzed using a Scanning Electron Microscope (SEM, JSM-6390 LV JEOL, 30 kV) coupled with EDS (Oxford Instruments X-Max^N).

The relative dielectric permittivity $\varepsilon_r(\omega)$ of $Ba(Zr_{0.10}Ti_{0.90})O_3$ was measured on disc samples using low-frequency impedance analyzer HP4119A and high-frequency impedance analyzer HP 4191A. First, the real and the imaginary part of impedance Z (ω) of disc samples were measured using measuring mode of parallel RC circuit. The obtained data were then used for calculating parallel capacitance Cp(ω) and parallel resistance Rp(ω). In the second step, the relative dielectric permittivity $\varepsilon_r(\omega)=\varepsilon_{r'}(\omega)+j\varepsilon_{r''}(\omega)$ was calculated using Cp and Rp.

3. Results and Discussion
3.1. Sintering

Fig. 1. shows relative densities of BZT samples sintered at 1100, 1200, and 1350^oC for different periods of sintering time. These results show: although the samples sintered at 1100^oC generally have lower relative densities than the samples sintered at 1200 ^oC for a time

_____

up to 40 minutes, after a sintering time of 120 minutes, there is no appreciable difference between sintering at 1100 and 1200°C respectively, as both samples achieved relative densities of around 65%. However, sintering at 1350°C achieved significantly higher relative densities of around 85-95% with a maximum relative density of 96% achieved for the samples mechanical activated for 120 minutes.
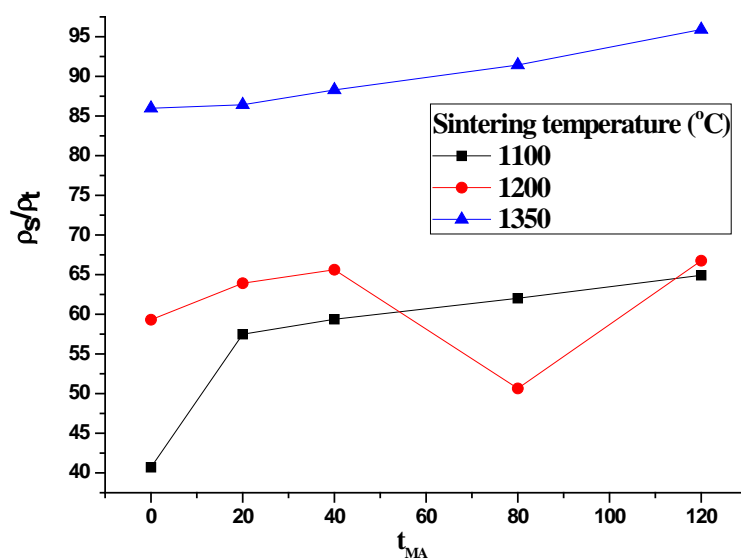
Fig. 1. Relative density dependence vs. sintering time of BZT samples sintered at different temperatures.

In the context of electrical properties, it is commonly accepted that samples with higher relative densities will exhibit superior electrical properties, primarily due to elimination of negative effects of grain boundaries, larger crystalline and grain size, and more compact structure.

3.2. Microstructure

The fractured surface reveals a densely packed granular microstructure (Fig. 2). It is well known that the sintering process favours an increase in number of large grains growing at the expense of fine grains of a strain-free matrix [55]. Growth terraces are visible on almost all the grains as evident from Fig. 2b indicating that grain growth might have occurred due to a layer mechanism probably on account of screw dislocations [56]. The appearance of domain structure in the high resolution SEM in these compounds was reported earlier [57]. In the present work also the domains are visible and can be seen from Fig. 2c. Wei Cai et al. reported that the strain energy as well as the depolarization energy can be reduced by the formation of 90° and 180° domains in case of small grains, whereas in case of large grains (>40 nm) the energy is reduced by formation of 180° domains [56]. The relative density of the BZT ceramics was found to be ~96 % of the theoretical density.

_____
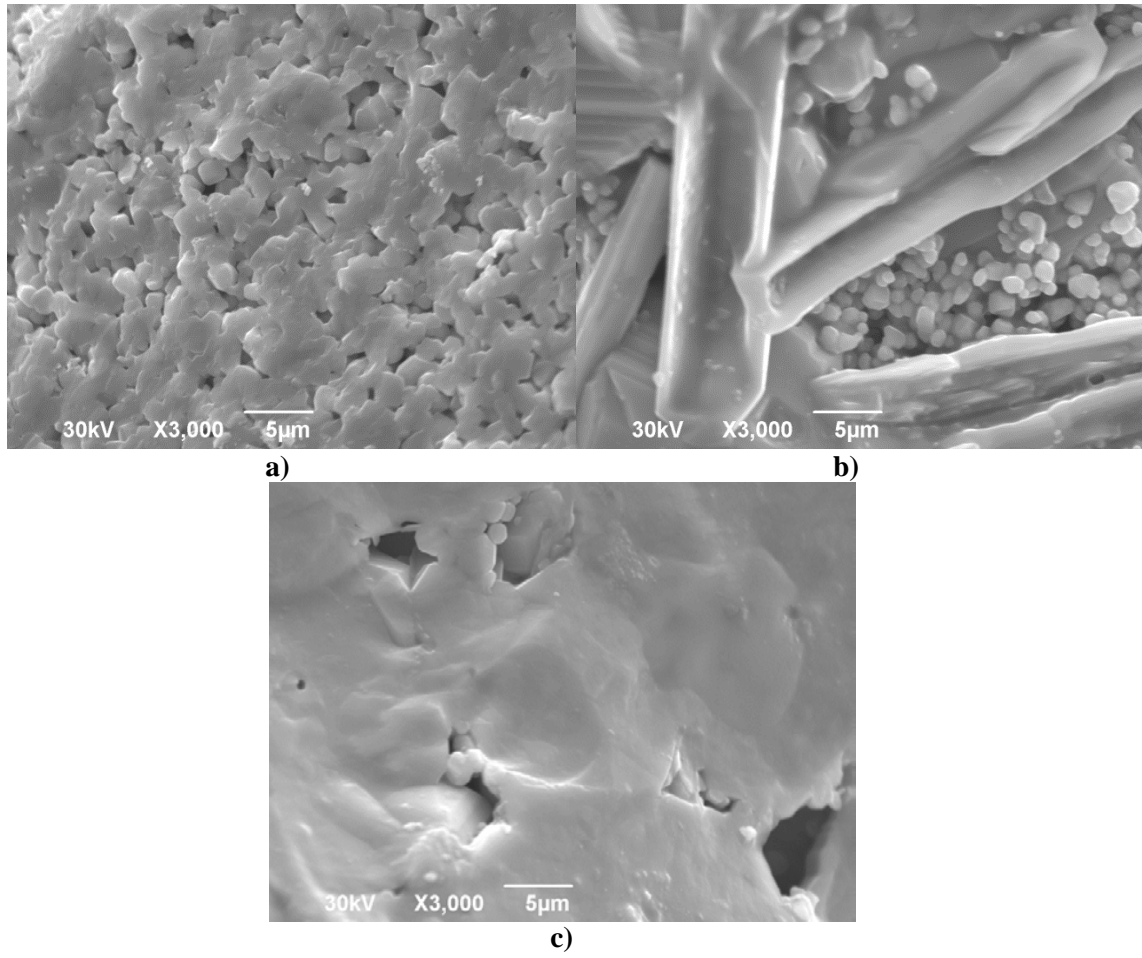
Fig.2. SEM images of a) BZT-S-0, b) BZT-S-80 and c) BZT-S-120 sintered at 1350°C.
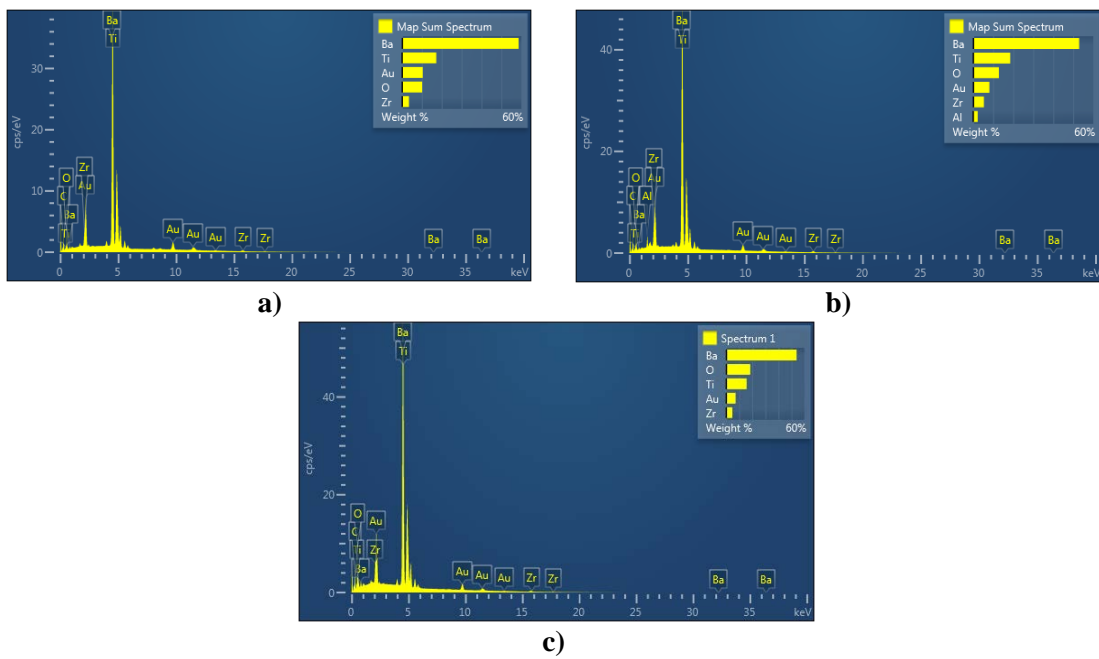
Fig. 3. EDS images of BZT ceramics sintered on 1350°C: a) 0 min, b) 80 min and c) 120 min.

_____

EDS analysis in Fig. 3. shows that zirconium is incorporated into the sample to a varying degree. However, this analysis only provides information on the local content in the sample and is not fully indicative of trends in the entire sample. Therefore, while we can conclude that zirconium has been incorporated into the sample, it is hard to determine the average zirconium content of individual samples based solely on EDS analysis.

Tab. I Microstructure parameters from XRD diffractometry.

Sample	a	c	Crystallite Size (nm)	Lattice Strain
BZT-120-1350	4.012 ± 0.001	4.020 ± 0.001	55 ± 2	0.021 ± 0.001
BZT-120-1200	4.03 ± 0.001	4.04 ± 0.001	40 ± 2	0.045 ± 0.001
BZT-120-1100	4.015 ± 0.001	4.053 ± 0.001	34 ± 2	0.120 ± 0.005
BZT-80-1350	4.0169 ± 0.001	4.007 ± 0.001	35 ± 2	0.041 ± 0.001
BZT-80-1200	4.0334 ± 0.001	3.997 ± 0.001	26 ± 2	0.044 ± 0.001
BZT-80-1100	4.0384 ± 0.001	4.0064 ± 0.001	18 ± 2	0.045 ± 0.001
BZT-40-1200	4.037 ± 0.001	4.0341 ± 0.001	61 ± 2	0.022 ± 0.001
BZT-40-1100	4.037 ± 0.001	4.0341 ± 0.001	36 ± 2	0.042 ± 0.001
BZT-20-1200	4.03 ± 0.001	4.03 ± 0.001	70 ± 2	0.05 ± 0.001
BZT-20-1100	4.022 ± 0.001	4.013 ± 0.001	21 ± 2	0.121 ± 0.005
BZT-0-1350	4.0281 ± 0.001	4.0153 ± 0.001	50 ± 2	0.022 ± 0.001
BZT-0-1200	4.0307 ± 0.001	4.0254 ± 0.001	29 ± 2	0.04 ± 0.001
BZT-0-1100	4.0236 ± 0.001	4.0118 ± 0.001	21 ± 2	0.05 ± 0.001

Table I shows microstructural parameters obtained from XRD analysis. The average crystalline size was determined using Debye-Scherer method [58] and Williamson-Hall method was used to calculate the microstrain [59].These results show that, in general, samples activated for 40 minutes exhibit the highest lattice volume-although the differences are within 1.3% of the volume of BZT-0-1100 sample, indicating relatively small changes due to the incorporation of zirconium into the lattice. Samples made of the powder activated for 80 and 120 minutes and sintered at 1350°C exhibit the lowest lattice volume, suggesting more uniform zirconium distribution in the grain. Also, samples activated for 120 minutes exhibit a/c of less than 1, while all other samples exhibit a/c over 1, suggesting that mechanical activation for 120 minutes incorporated the most zirconium into the BZT lattice, leading to shortening of the lattice along the c-axis, relative to the a-b plane.

Samples activated for 80 minutes exhibit the smallest average crystalline size, indicating that at higher activation time's agglomeration occurs leading to higher crystalline sizes in sintered samples activated at 120 minutes. As expected, the samples sintered at 1350°C generally exhibit the lowest microstrain, due to elimination of defects during sintering.

3.3. Impedance Spectroscopy

Since there is a significant difference in relative density and microstructure between samples sintered at 1100 and 1200°C, and samples sintered at 1350°C, respectively, only results for the best systems – those sintered at 1350°C are shown, because these were found to exhibit the best electrical properties.
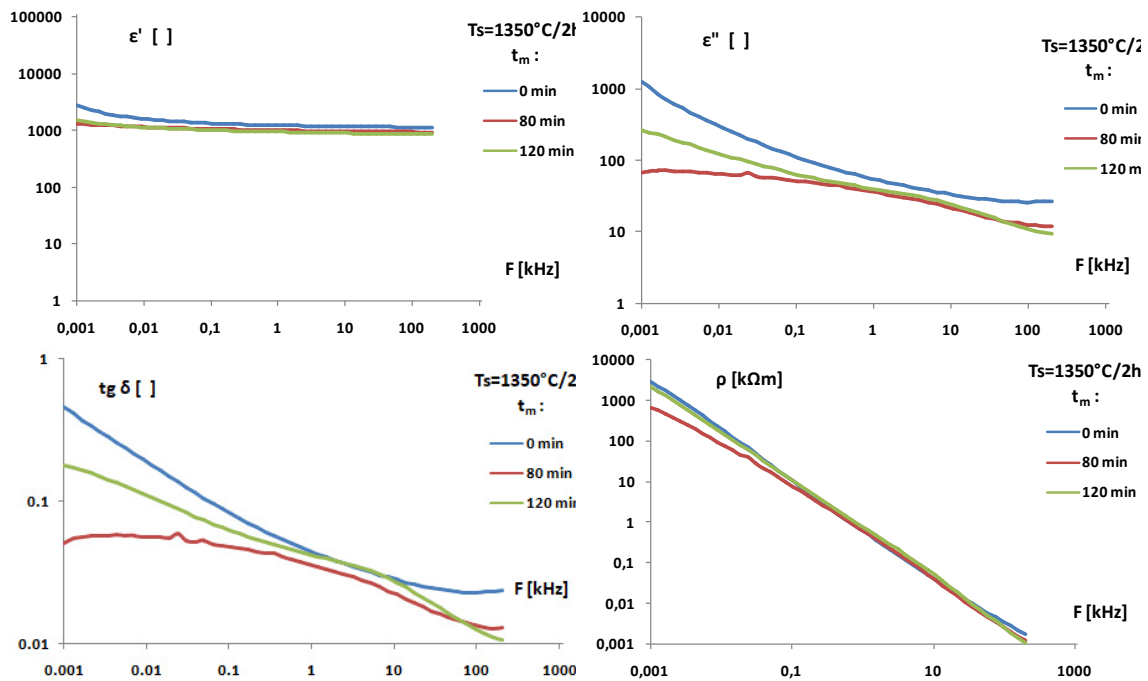
Fig. 3. Frequencies dependence of real and imaginary permittivity, tangent loss, and resistivity at different times of mechanical activation for the $Ba(Zr_{0.10}Ti_{0.90})O_3$ ceramic sintered at 1350^oC.

Fig. 3. shows the results of impedance spectroscopy for samples sintered at 1350^oC. These show that the tangent loss of samples sintered for 80 minutes is the lowest across the entire frequency range, while resistivity for these samples is significantly improved in the low frequency region. In addition, the samples sintered for 80 and 120 minutes exhibit very good stability of dielectric permittivity (ε') across the frequency range, while exhibiting significantly lower values of ε'' compared to non-sintered samples.

This can be attributed to larger grain size and more compact structure of sintered samples seen in the SEM analysis (Fig. 1). This increases the maximum transport path of the electron and reduces the negative effects of grain boundaries, where electron transport is slower. Overall, these effects reduce both resistivity and tangent loss, although sintering also results in a decrease of dielectric permittivity at lower frequencies. However, for application purposes, sintering improves general characteristics of BZT ceramics, and with sintering for 80 minutes provides optimal properties.

4. Conclusion

Mechanical activation of BZT ceramics precursor before sintering shows that relatively compact samples can be obtained at lower sintering temperatures, where samples with 85-95% relative density have been obtained after sintering at 1350^oC for 2 h. This is full 200 degrees lower that the typical BZT ceramics sintering temperature, which also takes from 2 to 8 h, anywhere [44-47], indicting significant technological potential of mechanical activation of precursors for preparation of BZT ceramics. Significantly lower sintering temperature and shorter sintering time would result in significant energy savings. In addition, microstructure analysis suggests that longer activation times lead to higher zirconium content in the final BZT ceramics.

_____

The samples mechanically activated for 80 and 120 minutes and sintered at 1350°C have also shown superior electrical properties to non-activated sample, as measured using impedance spectroscopy. They exhibit significantly lower resistivity and tangent loss, while maintaining relatively high and stable value of dielectric permittivity across the investigated frequency range. This suggests that mechanical activation is a viable method of producing high-performance BZT electroceramic materials at a lower cost.

Acknowledgments

5. References

1. Cross L. E., "Relaxer Ferroelectrics", Ferroelectrics, Vol. 76, No. 1 (2011) 241-267.
2. Bokov A. A. and Ye Z. G., J. Mater. Sci., 41 (2006) 31.
3. Sebastian M. T, Dielectric Materials for Wireless Communication (Amsterdam: Elsevier) chapter 3, pp 58, 2008.
4. Dimitrakopoulos C. D., Kymissis I, Purushothaman S, Neumayer D A, Duncombe P R and Laibowitz R B, Adv. Mater., 11 (1999) 1372.
5. Xu J, Menesklou W and Ivers-Tiff´ee E, J. Eur. Ceram. Soc. 25 (2005) 2289.
6. Xu J B, Zhai J W and Yao X, Ferroelectrics ,357 (2007) 730.
7. Bokov A A, Maglione M and Ye Z G,J. Phys., Condens. Matter, 19 (1999) 092001.
8. Gene H. Haertling, Ferroelectric Ceramics: History and Technology, J American Ceramic Society, (1999) 797-818.
9. Cai, W. FU, C. GAO, J. Chen, H. Effects of grain size on domain structure and ferroelectric properties of barium zirconate titanate ceramics, Journal of Alloys and Compounds, 480 (2009) 870-873.
10. Puli, V. S., Pradhan, D. K., Chrisey, D. B., Tomozawa, M., Sharma, G. L., Scott, J. F., Katiyar, R. S. Structure, dielectric, ferroelectric, and energy density properties of (1−x)BZT–xBCT ceramic capacitors for energy storage applications, J Mater Sci., 48 (2013) 2151-2157.
11. J. Bera and S.K. Rout On The Formation Of BaTiO$_3$- BaZrO$_3$ Solid Solution Through Solid-Oxide Reaction, Materials Letters, (2004) 135-138.
12. Yu, Z., Ang, C., Guo, R., Bhalla, A. S., Piezoelectric and strain properties of Ba(Ti$_{1-x}$Zr$_x$)O$_3$ceramics, J. Appl. Phys. 92 (2002) 1489-1493.
13. Maiti, T., Guo, R., Bhalla, A. S., Structure-Property Phase Diagram of BaZr$_x$Ti$_{1-x}$O$_3$, System, J American Ceramic Society, 91 (2008) 1769-1780.
14. D. Kosanović, N. J. Labus, J. Živojinović, A. Peleš Tadić, V. A. Blagojević, Vladimir B. Pavlović, Effects of mechanical activation on the formation and sintering kinetics of barium strontium titanate ceramics, Science of Sintering, 52 (4) (2020) 371-385.
15. D. A. Kosanović,V. A. Blagojević, N. J. Labus, N. B. Tadić, V. B. Pavlović, M. M. Ristić, Effect of Chemical Composition on Microstructural Properties and Sintering Kinetics of (Ba,Sr)TiO$_3$ Powders, Science of Sintering, 50(1) (2018) 29-38.

16. D. Kosanović, J. Živojinović, N. Obradović, V. P. Pavlović, V. B. Pavlović, A. Peleš, M. M. Ristić, The influence of mechanical activation on the electrical properties of $Ba_{0.77}Sr_{0.23}TiO_3$ ceramics, Ceramics International, 40, 8 Part A (2014) 11883-11888.

17. D. Kosanović, N. Obradović, J. Živojinović, S. Filipović, A. Maričić, V. Pavlović, Y. Tang, M. M. Ristić, Mechanical-Chemical Synthesis $Ba_{0.77}Sr_{0.23}TiO_3$, Science of Sintering, 44(1) (2012) 47-55.

18. J.G. Cheng, J. Tang, J.H. Chu, A.J. Zhang, Appl. Phys. Lett., 77 (2000) 1035.

19. J.H. Jeon, Y.D. Hahn, H.D. Kim, J. Eur. Ceram. Soc., 21 (2001) 1653-1656.

20. A. Catalan, S. Chang, R. Poisson, W. Baney, J. Benci, J. Mater. Res. 13 (1998) 1548-1552.

21. B. Baumert, L. Chang, A. Matsuda, C. Tracy, N. Cave, R. Gregory, P. Fejes, J. Mater. Res. 13 (1998) 197-204.

22. S. Nenez, A. Morell, M. Pate, M. Maglione, J. Niepce, J. Ganne, Eur. Ceram. 206 (2002) 1513.

23. D. Hennings, A. Schnell, G. Simon, J. Am. Ceram. Soc., 65 (1982) 539-544.

24. T. Maiti, R. Guo, A.S. Bhalla, J. Am. Ceram. Soc., 91 (2008) 1769-1780.

25. O.P. Thakur, C. Prakash, A.R. James, J. Alloys Comp., 470 (2009) 548-551.

26. N. Sawangwan, J. Barrel, K. Mackenzie, T. Tunkasiri, Appl. Phys. A: Mater. Sci. Process., 90 (2008) 723-727.

27. P. Ginet, C. Lucat, F. Ménil, Int. J. Appl. Ceram. Technol., 4 (5) (2007) 423-427.

28. Zhi Y, Chen A, Guo R and Bhalla A S, Appl. Phys. Lett. 81 (2002) 1285.

29. Tsurumi T, Yamamoto Y, Kakemoto H and Wada S, J. Mater. Res. 17 (2002) 755.

30. Ravez J, Broustera C and Simon A, J. Mater. Chem. 9 (1999) 1609.

31. Yu Z, Guo R and Bhalla A S, Appl. Phys. Lett., 77 (2000) 1535.

32. Qin W F, Xiong J, Zhu J, Tang J L, Jie W J, Zhang Y and Li Y R, J. Mater. Sci., 43 (2008) 409.

33. Y. Zhi, A. Chen, R. Guo, A.S. Bhalla, J. Appl. Phys. 92 (2002) 1489.

34. C.M. Wu, T.B. Wu, M.L. Chen, Appl. Phys. Lett. 69 (1996) 2659.

35. X.G. Tang, J. Wang, X.X. Wang, H.L.W. Chan, Sol. State Commun. 131 (2004) 163.

36. R.D. Weir, C.W. Nelson, US7033406B2, 2006.

37. P. Hansen, US006078494A, 2000.

38. J.Q. Qi, Z.L. Gui, Y.L. Wang, Q. Li, T. Li, L.T. Li, J. Mater. Sci. Lett. 21 (2002) 405.

39. H. Feng, J. Hou, Y. Qu, D. Shan, G. Yao, Structure, dielectric and electrical properties of cerium doped barium zirconium titanate ceramics, Journal of Alloys and Compounds, 512 (2012) 12-16.

40. W. Caia, C. Fu, J. Gao, H. Chen, Effects of grain size on domain structure and ferroelectric properties of barium zirconate titanate ceramics, Journal of Alloys and Compounds, 480 (2009) 870-873.

41. P. Arora Jha, A.K. Jha, Influence of processing conditions on the grain growth and electrical properties of barium zirconate titanate ferroelectric ceramics, Journal of Alloys and Compounds, 513 (2012) 580-585.

42. T. Badapanda, S. Sarangi, B. Behera, S. Anwar, Structural and impedance spectroscopy study of Samarium modified Barium Zirconium Titanate ceramic prepared by mechano-chemical route, Current Applied Physics, 14 (2014) 1192-1200.

43. S. Mahajan, D. Haridas, S. T. Ali, N. R. Munirathnam, K. Sreenivas, O. P. Thakur, Chandra Prakash, Investigation of conduction and relaxation phenomena in $BaZr_xTi_{1-x}O_3$ (x=0.05) by impedance spectroscopy, Physica B, 451 (2014) 114-119.

44. Dobal PS, Dixit A, Katiyar RS, Yu Z, Guo R, Bhalla AS., J Appl Phys, 89 (2001) 8085.

45. Yu Z, Ang C, Guo R, Bhalla AS., J Appl Phys,Ferroelectric-relaxor behavior of $Ba(Ti_{0.7}Zr_{0.3})O_3$ ceramics,92 (2002) 2655.

46. Tang XG, Chew KH, Chan HLW., Acta Mater, 52 (2004) 5177.

_____

47. Yu Z, Ang C, Guo R, Bhalla AS. Appl Phys Lett, Dielectric properties and high tunability of $Ba(Ti_{0.7}Zr_{0.3})O_3$ ceramics under dc electric field,81 (2002) 1285.

48. Bernardi, M. I. B.; Antonelli, E.; Lourenço, A. B.; Feitosa, C. A. C.; Maia, L. J. Q.; Hernandes, A. C. $BaTi_{1-x}Zr_xO_3$ nanopowders prepared by the modified Pechini method, J Therm Anal Calorim., 87 (2007) 725-730.

49. Yu, Z.; Guo, R.; Bhalla, A. S. Dielectric behavior of $Ba(Ti_{1-x}Zr_x)O_3$ single crystals, J. Appl. Phys., 88 (2000) 410.

50. C. Vasilescu, L. P. Curecheriu, L. Mitoseriu Phase Formation, Microstructure and Functional Properties Of Some BZT Ceramics, U.P.B. Sci. Bull. pp.65, 2015.

51. Tang, X. G.; Chew, K.-H.; Chan, H., Diffuse phase transition and dielectric tunability of $Ba(Zr_yTi_{1-y})O_3$ relaxor ferroelectric ceramics, Acta Materialia, 52 (2004) 5177-5183.

52. Rehrig, P. W.; Park, S.-E.; Trolier-McKinstry, S.; Messing, G. L.; Jones, B.; Shrout, T. R. Piezoelectric properties of zirconium-doped barium titanate single crystals grown by template grain growth, J. Appl. Phys.,86 (1999) 1657.

53. Dobal, P. S.; Dixit, A.; Katiyar, R. S.; Yu, Z.; Guo, R.; Bhalla, A. S. Micro-Raman scattering and dielectric investigations of phase transition behavior in the $BaTiO_3$–$BaZrO_3$ system, J. Appl. Phys.,89 (2001) 8085.

54. Yang, L.-J.; Wu, L.-Z.; Dong, S. First-principles study of the relaxor ferroelectricity of $Ba(Zr,Ti)O_3$, Chinese Phys. B.,24 (2015) 127702.

55. B. Garbarz-Glos, R. Bujakiewicz-Koronska, D. Majda, M. Antonova, A. Kalvane, C. Kus, Differential Scanning Calorimetry investigation of Phase transition in $BaZr_xTi_{1-x}O_3$, Integr. Ferroelectr. 108 (2009) 106-115.

56. Wei Cai, Fu Chunlin, Jiacheng Gao, Huaqiang Chen, Effects of grain size on domain structure and ferroelectric properties of barium zirconate titanate ceramics, J. Alloys Comp. 480 (2009) 870-873.

57. F. Moura, A. Z. Simoes, B. D. Stojanovic, M. A. Zaghete, E. Longoa, J. A. Varela, Dielectric and ferroelectric characteristics of barium zirconate titanate ceramics prepared from mixed oxide method, J. Alloys Comp. 462 (2008)129-134.

58. U. Holzwarth, N. Gibson, The Scherrer equation versus the'Debye-Scherrer equation'. Nature nanotechnology, 6(9) (2011) 534-534.

59. V.D.Mote, Y.Purushotham, B.N.Dole, Williamson-Hall analysis in estimation of lattice strain in nanometer-sized ZnO particles, Journal of theoretical and applied physics, 6 (2012)1-8.

_____

Сажетак: *БЗТ керамика је припремљена применом финог праха мешавине $BaCO_3$, TiO_2 и ZrO_2 у одговарајућем молском односу да би се формирао $Ba(Zr_{0.10}Ti_{0.90})O_3$ реакцијом у чврстом стању на повишеној температури. Припремљени BZT је млевен у планетарном кугличном млину од 0-120 мин да би се постигле различите врсте праха од микрона до честица нано величине. Након карактеризације праха XRD и СЕМ узорци су пресовани у облику диска и синтеровани на различитим температурама од 1100-1350°C на ваздуху. Синтеровани узорци су окарактерисани СЕМ и одређена је и представљена њихова густина и просечна величина зрна у зависности од температуре синтеровања и квалитета праха (време млевења). Након тога су сребрне епоксидне електроде нанесене на узорке синтерованих дискова. Капацитет узорка диска и отпорност мерени су у области ниске фреквенције од 1 Hz до 200 kHz коришћењем анализатора импедансе ниске фреквенције. Као параметри су коришћене температуре синтеровања и степен праха. Коначно, специфични отпор ρ, диелектрична константа (ε' + jε'') и tgδ су одређени из мерења импедансе. Анализирано је понашање електронских својстава, нпр. ефекат релаксације просторног набоја (међугрануларни*

_____

електрични набој) у зависности од температуре синтеровања и квалитета керамике Добијени резултати су упоређени са најбољим литературним подацима за губитке у BZT керамици на ниским фреквенцијама.
Кључне речи*: BZT керамика, синтеровање,диелектрична својства.*